JASA Express Letters

FEBRUARY 22 2022

Acoustic Luneburg lens based on a gradient metasurface for spoof surface acoustic waves

Yi Zheng; Shanjun Liang; Haiyan Fan; Shuowei An; Zhongming Gu; He Gao; Tuo Liu; Jie Zhu

JASA Express Lett. 2, 024004 (2022)
https://doi.org/10.1121/10.0009611

JASA EXPRESS LETTERS ARTICLE asa.scitation.org/journal/jel

Acoustic Luneburg lens based on a gradient metasurface for spoof surface acoustic waves

Yi Zheng,[1] Shanjun Liang,[2,a)] Haiyan Fan,[1] Shuowei An,[1] Zhongming Gu,[1,b)] He Gao,[1,c)] Tuo Liu,[1,d)] and Jie Zhu[3,e)]

[1]*Department of Mechanical Engineering, The Hong Kong Polytechnic University, Hung Hom, Kowloon, Hong Kong SAR, People's Republic of China*

[2]*Division of Science, Engineering and Health Studies, College of Professional and Continuing Education, Hong Kong Polytechnic University, Hong Kong SAR, People's Republic of China*

[3]*Institute of Acoustics, School of Physics Science and Engineering, Tongji University, Shanghai 200092, People's Republic of China*

yzheng254-c@my.cityu.edu.hk, junot.liang@cpce-polyu.edu.hk, hai-yan.fan@connect.polyu.hk, 19074539R@connect.polyu.hk, gzm989@gmail.com, he-e.gao@polyu.edu.hk, tuo.liu@connect.polyu.hk, jiezhu@tongji.edu.cn

Abstract: This letter presents the design and experimental demonstration of a gradient metasurface guiding spoof surface acoustic waves (SSAWs) in the manner of a Luneburg lens for sound. By correlating the propagation characteristics of SSAWs with the effective surface acoustic impedance, a straightforward concentric surface structure design is proposed to realize the required refractive index distribution. The results from both simulation and measurement show that grazing incident sound is converted into SSAWs propagating along the metasurface and focusing on the edge of the opposite side of the lens, which may find applications in direction detection and acoustic sensing.

[Editor: Vladimir E. Ostashev] https://doi.org/10.1121/10.0009611

Received: 5 January 2022 **Accepted:** 2 February 2022 **Published Online:** 22 February 2022

1. Introduction

Spoof surface acoustic waves (SSAWs) are a type of evanescent waves propagating over structured (e.g., perforated or grooved) surfaces and exhibiting compressed wavelength and structure-governed dispersion.[1–3] They have attracted increasing attention in the past decade and have been extensively investigated for various associated effects and functionalities such as extraordinary acoustic transmission,[4–6] beam collimation,[7,8] directional or anisotropic wave guiding,[9–12] and subwavelength focusing[13–16] and imaging.[17–19] Since the wave field of such airborne surface mode can be readily measured in a non-invasive manner, structures supporting SSAWs also appear as an ideal testbed for the direct observation of many intriguing physical phenomena.[11,20–25] In parallel, the possibility of adjusting the effective refractive index of SSAWs through engineering the surface building blocks have inspired a new direction towards subwavelength sound manipulation and gradient index (GRIN) design for acoustic waves. With a spatial variation of the building blocks, artificially structured surfaces, namely, the so-called GRIN metasurfaces for SSAWs, have been proved adequate to control SSAW propagation on demand, enabling innovative acoustic devices such as rainbow-trapping sensors,[26–28] a focusing lens,[16,29] a wave-based analogue computing device,[30] and vortex emitters.[31,32] Among various GRIN devices, the SSAW version of the Luneburg lens has not been realized so far.

The Luneburg lens was first proposed in geometrical optics[33] more than fifty years ago, in which the parallel rays of incident plane waves from one side are gradually bent to focus on the opposite edge of the circular or spherical lens. Soon afterwards, Boyles introduced this concept to an acoustic wave system.[34,35] However, the acoustic Luneburg lenses did not receive much attention until the emergence of acoustic artificial structures that allow flexible modulation of the required refractive index distribution. A series of GRIN metamaterials or phononic crystals have been utilized to realize acoustic Luneburg lenses for purposes of imaging,[36,37] signal retroreflection,[38] and ultra-long emission.[39] In this letter, we propose a surface-type acoustic Luneburg lens by modulating SSAWs with a gradient metasurface. The building blocks of the metasurface are graded perforations arranged in a concentric manner, in which the surface acoustic impedance of

[a)]ORCID: 0000-0003-2863-6441.
[b)]ORCID: 0000-0003-0865-540X.
[c)]ORCID: 0000-0001-8613-9959.
[d)]Author to whom correspondence should be addressed. Also at: The Hong Kong Polytechnic University Shenzhen Research Institute, Shenzhen 518057, People's Republic of China. ORCID: 0000-0002-5223-3258.
[e)]ORCID: 0000-0002-2547-7775.

each concentric layer is considered as a whole to achieve the lens design. We numerically and experimentally show that plane acoustic waves grazing the metasurface from various directions can be coupled to the SSAWs with trajectories converging at the outer boundary of the lens as expected, which can potentially be applied to directional detection and sensing.

2. Design methods of the SSAW Luneburg lens

A Luneburg lens exhibits spatially continuous variation of refractive index along the radial direction, expressed as $n = \sqrt{2-(r/R)^2}$, where R is the radius of the lens and r is the distance between an internal point and the center. Due to the lack of such materials in nature, discretization of the refractive index distribution is usually performed to facilitate the lens design.[38,40,41] For instance, one may allocate the specific refractive indices to individual concentric layers by taking advantage of the axial symmetry to create a graded refractive index profile.[42] By defining the effective radius of a layer as the arithmetic mean of its inner and outer radii,[43] the refractive index of a Luneburg lens can be rewritten in a discrete form,

$$n_i = \sqrt{2-\left(\frac{i-0.5}{N}\right)^2}, \tag{1}$$

where N is the total quantity of the concentric layers and i is a positive integer denoting a layer's sequence number from 1 to N.

For SSAWs, the designated distribution of refractive index can be realized by spatially varying the surface structures to form a gradient metasurface. Previously, the band structure of a square lattice was commonly used to determine the effective refractive index of SSAWs.[16,18,19,29,44,45] However, concerning the design of a circular lens, a large amount of square unit cells sufficiently small is needed to approximate the refractive index distribution and fit the curved edge.[32,36,37,42,46,47] Otherwise, the unit cells turn deformed in a cylindrical coordinate, which leads to inevitable deviation of the effective properties, especially near the coordinate origin.[38,48] To circumvent this issue, here we directly consider the overall surface acoustic impedance Z_s rather than the detailed structures during the derivation of the dispersion relation of SSAWs and the gradient metasurface design.

In the long-wavelength limit, the dispersion relation can be found by analyzing the divergence (zero of the denominator) of the reflection coefficient,[44,49] $R_p = (Z_s\cos\theta - \rho_0 c_0)/(Z_s\cos\theta + \rho_0 c_0)$, for a plane wave obliquely incident upon a flat surface of impedance Z_s, where ρ_0 and c_0 are the density and speed of sound in air, $k_0 = \omega/c_0$ is the wavenumber with ω being the angular frequency, θ denotes the angle of incidence with $\cos\theta = k_0^{-1}k_\perp = k_0^{-1}\sqrt{k_0^2 - k_\parallel^2}$, and $k_\perp$ and $k_\parallel$ are, respectively, the out-of-plane and in-plane wavevector components satisfying $k_\perp^2 + k_\parallel^2 = k_0^2$. A surface mode is propagative within the plane while evanescent along the vertical direction, which suggests $k_\parallel > k_0$ and imaginary $k_\perp$. Hence, by rewriting $k_\perp = j\sqrt{k_\parallel^2 - k_0^2}$ ($j = \sqrt{-1}$), the dispersion relation of SSAW is derived as

$$k_\parallel^2 + \left(\frac{Z_0^2}{Z_s^2} - 1\right)k_0^2 = 0, \tag{2}$$

in which $k_\parallel$ corresponds to the propagation constant of SSAW, $Z_0 = \rho_0 c_0$ represents the characteristic acoustic impedance in air (background medium), and Z_s should be a negative imaginary number (in the ideal lossless case) to guarantee the existence of this surface mode. The refractive index of SSAW is defined as $n = c_0/c_\parallel = k_\parallel/k_0$, relative to that of air. Thus, we can build a straightforward relation between Z_s and n:

$$\frac{Z_s}{Z_0} = \frac{-j}{\sqrt{n^2-1}}. \tag{3}$$

With Eq. (3), one may easily determine the surface impedance distribution required by a Luneburg lens for SSAWs. It can be practically implemented through graded subwavelength perforations (blind holes on a rigid surface) along the radial direction, arranged in a concentric layout, as shown in Fig. 1. Some important principles need to be considered during the metasurface design: (a) the thickness of each concentric layer should be sufficiently small so that the discrete refractive index distribution approximately mimics the continuous one; (b) the structural parameters (e.g., dimensions and spacing of the holes) should be in the subwavelength regime so that the effective impedance description is valid; (c) extremely narrow structures should be avoided to reduce the influence of thermo-viscous losses;[44,50] and (d) spatial variation in geometrics of the building blocks is gradual along the radial direction to minimize the slightly changed coupling among neighboring concentric layers.

In our proof-of-concept demonstration here, we set the operating frequency as 6000 Hz and discretize the Luneburg lens region of total radius 150 mm into 12 concentric layers each with a thickness of 12.5 mm. We adjust the structural parameters including hole diameter d_i, hole depth h_i, and quantity of holes Q_i to modulate the surface acoustic

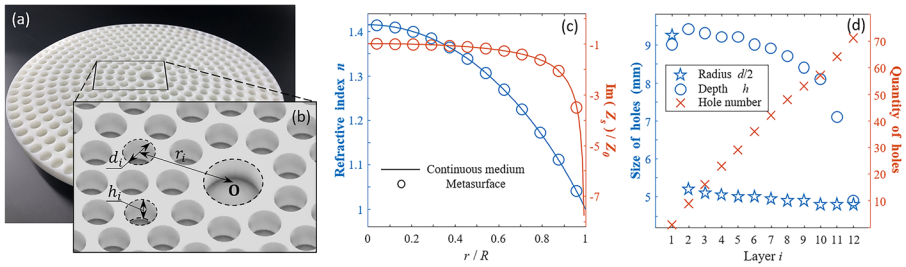

Fig. 1. Design of the Luneburg lens metasurface for SSAWs. (a) Photograph of the fabricated metasurface sample. The metasurface consists of 12 concentric layers with a total diameter of 300 mm. (b) Schematic illustration of the detailed geometries. Holes in each layer are uniformly arranged with diameter d_i and depth h_i, where i denotes the sequence number of the layers. r_i is the effective radius calculated as the arithmetic mean of the inner and outer radii of this layer. (c) Radial distributions of the refractive index and surface acoustic impedance in continuous and discrete forms. (d) Radial distribution of holes' geometries and quantity (see Table S1 in supplementary material for the detailed data list).

impedance of an individual concentric layer, where the subscript $i = 1, \ldots, 12$ denotes the layer number from the center. The effective surface impedance provided by the structures within an individual concentric layer can be numerically extracted and optimized in the commercial finite-element solver COMSOL MULTIPHYSICS. During the simulations, the target concentric layer (having identical and equally spaced holes) is mounted at the end of a virtual impedance tube with the corresponding ring-shaped cross-sectional area (except for the central one which is of circular cross section) so that the overall effective surface impedance is retrieved from the reflection coefficient under normal plane wave incidence.[51] The target effective property distributions as well as the associated structural parameters of our design are shown in Figs. 1(c) and 1(d), which are determined after a careful consideration of above-mentioned design principles and discussions about the discretization scheme and influence of losses.[51]

3. Results and discussions

We perform both 3D full-wave numerical simulations and experimental measurements to validate our design. For the simulations, the physical properties of air at 20 °C are $\rho_0 = 1.204\,\mathrm{kg/m^3}$, and $c_0 = 343.2\,\mathrm{m/s}$, and the computational domain is truncated with perfectly matched layers to eliminate unwanted reflections. The thermo-viscous losses inside the holes are taken into account to make the results more realistic. The corresponding measurements were conducted in an anechoic chamber as shown in Fig. 2. The 3D-printed metasurface sample (made of photosensitive resin) is placed horizontally in the middle of a square area with the side length of 330 mm for sound field scanning [see Fig. 2(a)]. A single loudspeaker is located 1.8 m away from the metasurface sample, generating continuous sinusoidal acoustic waves with nearly planar wavefront when approaching and grazing the sample, during which three representative azimuthal directions of incidence, $\phi = 0°$, 15°, and 30° are considered [see Fig. 2(b)]. A 1/4-in., preamplifier built-in free-field microphone (Brüel & Kjær, type 4935 together with a conditioning amplifier Brüel & Kjær, NEXUS type 2693 A) carried by a 2D linear stage was used to scan the sound fields 15-mm above the metasurface with a step of 5 mm along both the x and y directions. The signal generation and data acquisition is controlled by a lock-in amplifier (Zurich Instrument HF2LI).

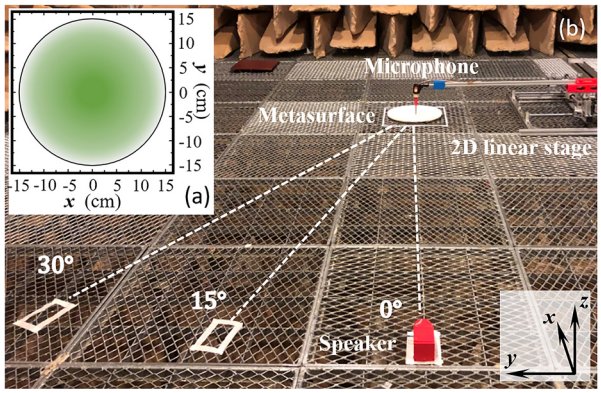

Fig. 2. Experimental setup. (a) Top view of the square scanning region. The color scale of the inset schematically illustrates the gradient distribution of the refractive index along the metasurface, with the darker green indicating larger refractive index at the center and the lighter green indicating smaller refractive index at the edge. (b) Scanning measurements in an anechoic chamber. The loudspeaker is arranged in the same horizontal plane with the metasurface sample to generate grazing incidence.

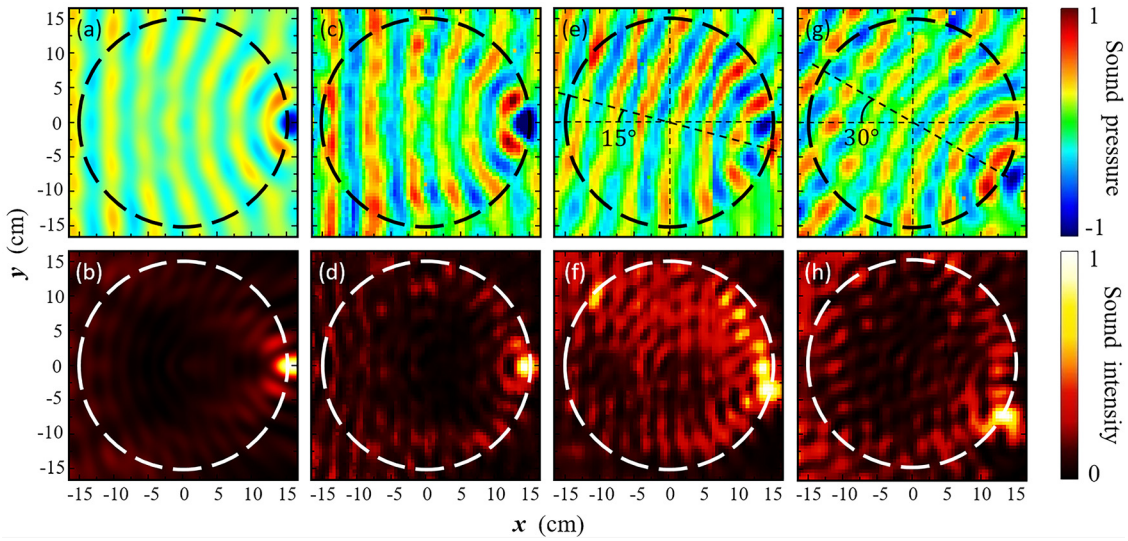

Fig. 3. Focusing effect of the SSAW Luneburg lens. (a), (b) Simulated sound fields 15-mm above the metasurface for incident azimuthal angle $\phi = 0°$. (c), (d) Corresponding experimental results. (e), (f) Experimental results for $\phi = 15°$. (g), (h) Experimental results for $\phi = 30°$. (a), (c), (e), and (g) are the normalized sound pressure fields, while (b), (d), (f) and (h) are the normalized sound intensity fields.

The numerical and experimental results at the incident azimuthal angle $\phi = 0°$ are shown in Figs. 3(a)–3(d), exhibiting a good agreement with each other. It can be observed that incident acoustic waves grazing the metasurface are converted into the SSAW mode guided by the gradient surface structures. The trajectories as indicated by the bending wavefront gradually converge towards a point on the edge of the circular lens, forming an energy hotspot of SSAWs on the opposite side of the incidence. As shown in Figs. 3(e)–3(h), when ϕ is changed from 0° to 15° and 30°, the location of the focal spot moves accordingly along the edge of the metasurface, in response to the direction of incidence. These results confirm the capability of the gradient metasurface to work as an acoustic Luneburg lens to detect the direction of incoming waves. In practice, by further embedding a microphone array along the circular edge of the metasurface, the directional information of sound sources can be inferred from the remarkable leaps of the captured signals.

Due to the dispersive behavior of SSAWs, the refractive index distribution is frequency-dependent and inevitably deviates away from that of a Luneburg lens at frequencies other than 6000 Hz. To evaluate the dispersion and broadband performance of the metasurface, we calculate the effective refractive index distributions at several different frequencies as given by Fig. 4(a), in which the inherent thermo-viscous losses inside the holes are also considered. At the designed operating frequency 6000 Hz, the refractive index profile almost overlaps with that of an ideal Luneburg lens despite a very slight deviation caused by the inherent losses. The variation of the curve caused by a frequency shift is more remarkable near the metasurface center while less on the edge. Such refractive index profile change leads to varied focal position along

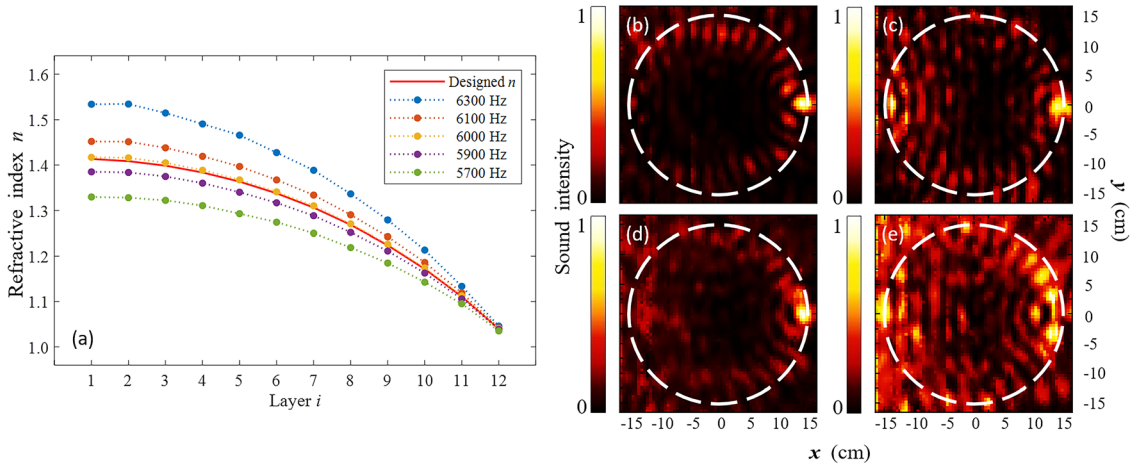

Fig. 4. Dispersion and broadband performance of the metasurface. (a) Distribution of the effective refractive index at different frequencies. (b)–(e) Experimentally measured sound intensity fields at 6300, 6100, 5900, and 5700 Hz, respectively.

the radial direction and declined performance but is still acceptable in terms of the focusing effect as long as the frequency shift is relatively small (e.g., ±100–200 Hz). We also examine the measured results at these frequencies for $\phi = 0°$. As shown in Figs. 4(b)–4(e), the focal spot moves inward or outwards along the x axis for a higher or lower operating frequency, as a result of the increased or decreased refractive index.[52] It is worth noting that the sound fields at lower frequencies [Figs. 4(d)–4(e)] are somewhat distorted compared to those at higher frequencies [Figs. 4(b)–4(c)]. This is due to the fact that the SSAW mode tends to be confined to the metasurface and dominate the near-field region when the frequency approaches the resonance of the surface structures from below. Detailed experimental results from 6500 Hz to 5600 Hz are also provided.[51]

4. Conclusion

In summary, we have presented the design and experimental realization of an acoustic Luneburg lens through a gradient metasurface for SSAWs with concentrically arranged building blocks. The effective surface acoustic impedance of each concentric layer is used to facilitate the design in polar coordinates, which is also applicable to other cylindrical lens design. The enhanced SSAW field that is confined to the structure and open to the ambience allows our direct experimental observation of the focusing process inside the Luneburg lens, with results agreeing well with the numerical simulations. With the capability to convert the incident plane waves into SSAWs and then focus them at a specific azimuthal location on the rim, the proposed metasurface could find applications in directional acoustic sensing and detection.

Acknowledgments

This work was supported by Internal Research Fund of The Hong Kong Polytechnic University (Grant No. ZZLC), Research Grants Council of the Hong Kong Special Administrative Region, China (Project Nos. PolyU 15219221 and PolyU 15205219), and National Natural Science Foundation of China (Grant Nos. 12104383 and 11774297).

References and links

[1]L. Kelders, J. F. Allard, and W. Lauriks, "Ultrasonic surface waves above rectangular-groove gratings," J. Acoust. Soc. Am. **103**(5), 2730–2733 (1998).
[2]Z. He, H. Jia, C. Qiu, Y. Ye, R. Hao, M. Ke, and Z. Liu, "Nonleaky surface acoustic waves on a textured rigid surface," Phys. Rev. B **83**(13), 132101 (2011).
[3]L. Quan, F. Qian, X. Liu, X. Gong, and P. A. Johnson, "Mimicking surface plasmons in acoustics at low frequency," Phys. Rev. B **92**(10), 104105 (2015).
[4]M. Lu, X. Liu, L. Feng, J. Li, C. Huang, Y. Chen, Y. Zhu, S. Zhu, and N. Ming, "Extraordinary acoustic transmission through a 1D grating with very narrow apertures," Phys. Rev. Lett. **99**(17), 174301 (2007).
[5]J. Christensen, L. Martin-Moreno, and F. J. Garcia-Vidal, "Theory of resonant acoustic transmission through subwavelength apertures," Phys. Rev. Lett. **101**(1), 014301 (2008).
[6]Z. Hou, X. Fang, Y. Li, and B. Assouar, "Highly efficient acoustic metagrating with strongly coupled surface grooves," Phys. Rev. Appl. **12**(3), 034021 (2019).
[7]J. Christensen, A. Fernandez-Dominguez, F. De Leon-Perez, L. Martin-Moreno, and F. Garcia-Vidal, "Collimation of sound assisted by acoustic surface waves," Nat. Phys. **3**(12), 851–852 (2007).
[8]Y. Zhou, M. Lu, L. Feng, X. Ni, Y. Chen, Y. Zhu, S. Zhu, and N. Ming, "Acoustic surface evanescent wave and its dominant contribution to extraordinary acoustic transmission and collimation of sound," Phys. Rev. Lett. **104**(16), 164301 (2010).
[9]J. Lu, C. Qiu, M. Ke, and Z. Liu, "Directional excitation of the designer surface acoustic waves," Appl. Phys. Lett. **106**(20), 201901 (2015).
[10]L. Quan and A. Alù, "Hyperbolic sound propagation over nonlocal acoustic metasurfaces," Phys. Rev. Lett. **123**(24), 244303 (2019).
[11]Y. Long, H. Ge, D. Zhang, X. Xu, J. Ren, M. Lu, M. Bao, H. Chen, and Y. Chen, "Symmetry selective directionality in near-field acoustics," Natl. Sci. Rev. **7**(6), 1024–1035 (2020).
[12]S. Yves and A. Alù, "Extreme anisotropy and dispersion engineering in locally resonant acoustic metamaterials," J. Acoust. Soc. Am. **150**(3), 2040–2045 (2021).
[13]F. Lemoult, M. Fink, and G. Lerosey, "Acoustic resonators for far-field control of sound on a subwavelength scale," Phys. Rev. Lett. **107**(6), 064301 (2011).
[14]X. Zhou, M. Badreddine Assouar, and M. Oudich, "Subwavelength acoustic focusing by surface-wave-resonance enhanced transmission in doubly negative acoustic metamaterials," J. Appl. Phys. **116**(19), 194501 (2014).
[15]A. Maznev, G. Gu, S. Sun, J. Xu, Y. Shen, N. Fang, and S. Zhang, "Extraordinary focusing of sound above a soda can array without time reversal," New J. Phys. **17**(4), 042001 (2015).
[16]T. Liu, F. Chen, S. Liang, H. Gao, and J. Zhu, "Subwavelength sound focusing and imaging via gradient metasurface-enabled spoof surface acoustic wave modulation," Phys. Rev. Appl. **11**(3), 034061 (2019).
[17]H. Jia, M. Ke, R. Hao, Y. Ye, F. Liu, and Z. Liu, "Subwavelength imaging by a simple planar acoustic superlens," Appl. Phys. Lett. **97**(17), 173507 (2010).
[18]J. Zhu, J. Christensen, J. Jung, L. Martin-Moreno, X. Yin, L. Fok, X. Zhang, and F. Garcia-Vidal, "A holey-structured metamaterial for acoustic deep-subwavelength imaging," Nat. Phys. **7**(1), 52–55 (2011).
[19]H. Jia, M. Lu, Q. Wang, M. Bao, and X. Li, "Subwavelength imaging through spoof surface acoustic waves on a two-dimensional structured rigid surface," Appl. Phys. Lett. **103**(10), 103505 (2013).

[20]D. Torrent and J. Sánchez-Dehesa, "Acoustic analogue of graphene: Observation of Dirac cones in acoustic surface waves," Phys. Rev. Lett. **108**(17), 174301 (2012).
[21]Y. Peng, C. Qin, D. Zhao, Y. Shen, X. Xu, M. Bao, H. Jia, and X. Zhu, "Experimental demonstration of anomalous Floquet topological insulator for sound," Nat. Commun. **7**(1), 13368 (2016).
[22]L. Wu, M. Oudich, W. Cao, H. Jiang, C. Zhang, J. Ke, J. Yang, Y. Deng, Q. Cheng, and T. Cui, "Routing acoustic waves via a metamaterial with extreme anisotropy," Phys. Rev. Appl. **12**(4), 044011 (2019).
[23]Z. Zhang, Y. Gu, H. Long, Y. Cheng, X. Liu, and J. Christensen, "Subwavelength acoustic valley-Hall topological insulators using soda cans honeycomb lattices," Research **2019**, 5385763.
[24]H. Ge, X. Xu, L. Liu, R. Xu, Z. Lin, S. Yu, M. Bao, J. Jiang, M. Lu, and Y. Chen, "Observation of acoustic skyrmions," Phys. Rev. Lett. **127**(14), 144502 (2021).
[25]S. Yves, R. Fleury, F. Lemoult, M. Fink, and G. Lerosey, "Topological acoustic polaritons: Robust sound manipulation at the subwavelength scale," New J. Phys. **19**(7), 075003 (2017).
[26]J. Zhu, Y. Chen, X. Zhu, F. J. Garcia-Vidal, X. Yin, W. Zhang, and X. Zhang, "Acoustic rainbow trapping," Sci. Rep. **3**(1), 17285 (2013).
[27]Y. Chen, H. Liu, M. Reilly, H. Bae, and M. Yu, "Enhanced acoustic sensing through wave compression and pressure amplification in anisotropic metamaterials," Nat. Commun. **5**(1), 5247 (2014).
[28]H. Jia, M. Lu, X. Ni, M. Bao, and X. Li, "Spatial separation of spoof surface acoustic waves on the graded groove grating," J. Appl. Phys. **116**(12), 124504 (2014).
[29]Y. Ye, M. Ke, Y. Li, T. Wang, and Z. Liu, "Focusing of spoof surface-acoustic-waves by a gradient-index structure," J. Appl. Phys. **114**(15), 154504 (2013).
[30]C. Yang, T. Liu, J. Zhu, J. Ren, and H. Chen, "Surface-acoustic-wave computing of the Grover quantum search algorithm with metasurfaces," Phys. Rev. Appl. **15**(4), 044040 (2021).
[31]J. Liu, B. Liang, and J. Cheng, "Focusing a two-dimensional acoustic vortex beyond diffraction limit on an ultrathin structured surface," Phys. Rev. Appl. **15**(1), 014015 (2021).
[32]S. Gao, Y. Li, C. Ma, Y. Cheng, and X. Liu, "Emitting long-distance spiral airborne sound using low-profile planar acoustic antenna," Nat. Commun. **12**(1), 2006 (2021).
[33]R. K. Luneburg, *Mathematical Theory of Optics* (University of California Press, Berkeley, 1964).
[34]C. Boyles, "Wave theory of an acoustic Luneberg lens," J. Acoust. Soc. Am. **43**(4), 709–715 (1968).
[35]C. Boyles, "Wave theory of an acoustic Luneburg lens. II. The theory of variable density lenses," J. Acoust. Soc. Am. **45**(2), 356–364 (1969).
[36]Y. Xie, Y. Fu, Z. Jia, J. Li, C. Shen, Y. Xu, H. Chen, and S. A. Cummer, "Acoustic imaging with metamaterial Luneburg lenses," Sci. Rep. **8**(1), 16188 (2018).
[37]J. W. Kim, S. J. Lee, J. Y. Jo, S. Wang, and S. H. Kim, "Acoustic imaging by three-dimensional acoustic Luneburg meta-lens with lattice columns," Appl. Phys. Lett. **118**(9), 091902 (2021).
[38]Y. Fu, J. Li, Y. Xie, C. Shen, Y. Xu, H. Chen, and S. A. Cummer, "Compact acoustic retroreflector based on a mirrored Luneburg lens," Phys. Rev. Mater. **2**(10), 105202 (2018).
[39]C. Lu, R. Yu, Q. Ma, K. Wang, J. Wang, and D. Wu, "GRIN metamaterial generalized Luneburg lens for ultra-long acoustic jet," Appl. Phys. Lett. **118**(14), 144103 (2021).
[40]S. Liang, T. Liu, H. Gao, Z. Gu, S. An, and J. Zhu, "Acoustic metasurface by layered concentric structures," Phys. Rev. Res. **2**(4), 043362 (2020).
[41]T. Chang, G. Dupont, S. Enoch, and S. Guenneau, "Enhanced control of light and sound trajectories with three-dimensional gradient index lenses," New J. Phys. **14**(3), 035011 (2012).
[42]J. Dockrey, M. J. Lockyear, S. Berry, S. Horsley, J. R. Sambles, and A. P. Hibbins, "Thin metamaterial Luneburg lens for surface waves," Phys. Rev. B **87**(12), 125137 (2013).
[43]S. H. Kim, presented at the *2014 8th International Congress on Advanced Electromagnetic Materials in Microwaves and Optics* (2014).
[44]T. Liu, S. Liang, F. Chen, and J. Zhu, "Inherent losses induced absorptive acoustic rainbow trapping with a gradient metasurface," J. Appl. Phys. **123**(9), 091702 (2018).
[45]M. Badreddine Assouar and M. Oudich, "Dispersion curves of surface acoustic waves in a two-dimensional phononic crystal," Appl. Phys. Lett. **99**(12), 123505 (2011).
[46]L. Zhao, T. Horiuchi, and M. Yu, "Broadband acoustic collimation and focusing using reduced aberration acoustic Luneburg lens," J. Appl. Phys. **130**(21), 214901 (2021).
[47]S. Tol, F. Degertekin, and A. Erturk, "Phononic crystal Luneburg lens for omnidirectional elastic wave focusing and energy harvesting," Appl. Phys. Lett. **111**(1), 013503 (2017).
[48]D. Schurig, J. J. Mock, B. Justice, S. A. Cummer, J. B. Pendry, A. F. Starr, and D. R. Smith, "Metamaterial electromagnetic cloak at microwave frequencies," Science **314**(5801), 977–980 (2006).
[49]F. Garcia-Vidal, L. Martin-Moreno, and J. Pendry, "Surfaces with holes in them: New plasmonic metamaterials," J. Opt. A-Pure Appl. Opt. **7**(2), S97 (2005).
[50]L. Schwan, A. Geslain, V. Romero-García, and J.-P. Groby, "Complex dispersion relation of surface acoustic waves at a lossy metasurface," Appl. Phys. Lett. **110**(5), 051902 (2017).
[51]See supplementary material at https://www.scitation.org/doi/suppl/10.1121/10.0009611 for the geometric parameters of the metasurface, the numerical simulation of continuous and discrete lenses, further discussion about the inherent thermo-viscous losses, and the, results of the broadband experiments.
[52]R. Fuentes-Domínguez, M. Yao, A. Colombi, P. Dryburgh, D. Pieris, A. Jackson-Crisp, D. Colquitt, A. Clare, R. J. Smith, and M. Clark, "Design of a resonant Luneburg lens for surface acoustic waves," Ultrasonics **111**, 106306 (2021).